Iraqi Journal of Physics, 2025
https://doi.org/10.30723/ijp.v23i3.1395

Vol.23, No.3, PP. 75-85
P-ISSN: 2070-4003
E-ISSN: 2664-5548

Investigation of Optical and Electrical Properties of Solid Polymer Electrolyte based on Natural Polymer

Alaa Munaf Qusay[1] and Mohammed Kadhim Jawad[1*]
Department of Physics, College of Science, University of Baghdad, Baghdad, Iraq
[*]Corresponding author: mohamedkadhom66@gmail.com

Abstract

Solid biopolymer electrolytes (SBEs) consisting of a natural blend that is leak-proof, biodegradable, and flexible are widely studied. In this study, SBE was prepared using the solution casting technique, consisting of a fixed 50:50 ratio of chitosan to polyvinylpyrrolidone (CS: PVP) and varying weight percentages of potassium iodide (KI) at 7.5, 15, 22.5, 30, and 37.5 wt%. The samples were characterized using UV-Vis spectrophotometry, Fourier transform infrared (FTIR), and AC conductivity. FTIR analysis showed that the polymer blend of CS: PVP interacted with the potassium salt. The addition of KI was found to disrupt hydrogen bonding between the polymer chains, likely due to the polymer-salt interaction. Only one absorption peak was observed in the UV-Vis spectroscopy of the sample at around 315 nm. The conductivity went up as the amount of KI increased, reaching a value of 3×10^{-4} S.cm^{-1} at room temperature for the CS: PVP blend with 37.

Article Info.

Keywords:
Biopolymer Mixture, Potassium Iodide Salt (KI), Optical Properties (UV/VIS), AC-Conductivity, Solid Biopolymer Electrolytes (SBEs).

Article history:
Received:Nov. 06, 2024
Revised: Feb. 11, 2025
Accepted:Feb. 24, 2025
Published:Sep. 01, 2025

1. Introduction

Sensors, high-density batteries such as Lithium-Ion Batteries (LIBs), electrochromic windows and displays, and photovoltaic cells have all benefited greatly from the advent of Solid Polymer Electrolyte (SPE) in recent years due to their adaptability, electrochemical stability, longevity, and safety [1]. The LIBs, with their high operating voltage, excellent cycle stability, and high energy density, have found widespread use in electric vehicles, grid storage systems, and portable electronic devices [2,3]. However, LIBs are highly combustible, explosive, and volatile, making their usage in large quantities a potential safety risk, particularly in applications such as energy storage power stations or electric vehicles [4,5]. Switching to Solid State Electrolytes (SPEs) from organic liquid electrolytes can eliminate the safety concerns and create LIBs with a high energy density employing large-capacity cathodes and lithium metal anodes. Eliminating polymer separators is another way to streamline the LIB production process [6]. Natural SPE preparation uses various host polymers, including biopolymers such as chitosan and its derivatives, starch, cellulose, and polylactic acid. Examples of synthetic polymers are vinyl chloride, polycarbonate, polyvinylidene fluoride, polyacrylonitrile, and polyethylene. The environmental friendliness, biocompatibility, abundance of natural sources, nontoxicity, readily availability, minimal cost of production, and exceptionally high mechanical and electrical properties are just a few of the reasons why electrolytes based on natural or biopolymers have drawn more attention from researchers [7-9]. The primary obstacle in developing SPEs is enhancing their ionic conductivity

© 2025 The Author(s). Published by College of Science, University of Baghdad. This is an open-access article distributed under the terms of the Creative Commons Attribution 4.0 International License (https://creativecommons.org/licenses/by/4.0/).

to match that of liquid electrolytes. Several methods are employed to address this challenge, including polymer blending, plasticization, copolymerization, and the addition of nanofillers. Over the past few decades, SPEs have been prepared based on biopolymers like chitosan, corn starch, carrageenan, agar-agar, and methylcellulose, which have exhibited the highest ionic conductivity at room temperature [10]. Chitosan (CS), derived from the world's second most abundant biopolymer, cellulose being the first, stimulated the curiosity of researchers seeking to create innovative and environmentally friendly products. The fact that it is inexpensive further adds to its merit as a material [11]. While offering several advantages and unique properties, chitosan films are limited by certain disadvantages. These include poor barrier properties against water vapor and gases, and poor mechanical and thermal performance, which restrict their broader applications. Polymer blending offers a promising solution to these limitations, providing an effective method for tailoring film characteristics to meet specific requirements [12]. Polyvinyl pyrrolidone (PVP) compounds merit consideration as a surface stabilizer and growth modulator. The carbonyl, amine, and alkyl groups are only a few functional groups found in PVP materials. The polar nitrogen and oxygen atoms constituting PVP's amine group have a strong attraction for metallic ions. These factors facilitate the association with metal atoms, enhancing the nucleus formation probability. PVP can be dissolved in water- and non-water-based solutions because it has a hydrophilic pyrrolidone moiety and a strong hydrophobic alkyl group [13]. Frequently, polymer salt complexes are produced by dispersing a trace amount of salt, such as potassium iodide (KI), in the respective solvent with the host polymer, which alters the ionic conductivity of the polymer [14,15]. Potassium iodide (KI) salt has been employed to regenerate the oxidized electrolyte and provide mobile ions. In contrast, the inorganic salt's poor solubility at room temperature is a prevalent drawback [16].

This work focuses on the effect of the KI on the optical and AC conductivity of solid biopolymer blend electrolytes. Chitosan was used as a natural, environmentally friendly polymer, making it an alternative to the chemicals used in batteries. When mixed with other materials, it shows a good ability to transport ions inside the battery and improves charging and discharging efficiency.

2. Experimental Procedures

2.1 Materials

Chitosan, of molecular weight and 75–85% deacetylation degree, with the chemical formula $(C_2H_4O)_n$, was supplied from the exporter's laboratory compounds (Himedia). It was used to obtain an extra purified product with a deacetylation degree of 86%. Polyvinylpyrrolidone (molecular weight of 40.000 and purity> 99%) and Potassium Iodide of molecular weight of 166.0028 g/mol were acquired from Sigma Aldrich Chemicals Ltd., India. Iodine (I_2) of 253.81 g/mol molecular weight was obtained from BDH Limited Poole, England.

2.2 Preparation

The films were fabricated utilizing a solution-casting procedure. The basic chitosan solution was produced by dissolving 0.5 g of CS in 40 mL of distilled water that contained 1% acetic acid. The mixture was then heated to 50°C and continuously stirred with a magnetic stirrer for approximately 5 hrs. 0.5 g PVP polymer, at a temperature of 25°C, was dissolved in 5 mL of distilled water that contained 1% acetic acid. The PVP solution was added to the CS solution at a 50:50 ratio and agitated continuously for two hours until a homogeneous aqueous solution was achieved. The solution was then poured into a plastic Petri dish. The same procedures were

repeated to prepare films with varying KI salt and I_2 ratios, as illustrated in Table 1. The iodine and KI were dissolved in 3 ml of dimethyl sulfoxide (DMSO), and the resulting mixture was gradually added to the CS: PVP polymer blend. The mixture was stirred for 2 hrs. Finally, to generate a dry, self-supporting film, the solution mixture was poured into several clean, dry plastic Petri dishes and vaporized gradually at 25° C.

Table 1: Structure of the prepared solid electrolytes.

Assignment	CS: PVP	KI wt%	KI g	I_2 g
A0 (pure)	50:50	0	0.0000	0.0000
A1	50:50	7.5	0.075	0.0115
A2	50:50	15	0.15	0.0229
A3	50:50	22.5	0.225	0.0344
A4	50:50	30	0.3	0.0459
A5	50:50	37.5	0.375	0.0573

3. Results and Discussion

3.1 Fourier Transform Infrared (FTIR)

The FTIR is a potent instrument in the field of polymer composite chemistry, capable of determining the specific chemicals as well as the framework's configuration [17]. The FTIR analysis facilitated the identification and investigation of the structural and compositional modifications in the SPE samples that occurred as a result of the addition and mixing of the dopant salt. The stretching or bending vibrational frequencies of a specific bond in a solid polymer electrolyte sample may be influenced by the local molecular interactions between the composite polymers and their complexation with the dopant salt [18]. Fig.1 shows The FTIR transmittance spectra of the CS: PVP blend demonstrated in the 400–4000 cm^{-1} range. Chitosan exhibits bands at 3261.63 cm^{-1} for –OH and –NH. These bands shifted to higher frequencies upon the incorporation of PVP to produce a polymeric blend [19]. The C-H_2 stretching vibration (methyl group) was represented by the conspicuous peaks at 2926.01 cm^{-1} [20]. The characterized band of chitosan located at 1647.21 cm^{-1} suggests that hydrogen bonds may exist between PVP and CS. The peak at 1647.21 cm^{-1} indicates stretching vibration of the carbonyl set C=O. Additionally, the CH_2 alteration phases of the CH_2 group have peaks at 1421.54 cm^{-1} and 1371.39 cm^{-1} [21]. It was confirmed that the amine group was present in the membrane matrix by the peak at 1282.66-1371.39 cm^{-1}, which was attributed to the C–N vibrating extending vibration, and C-N oscillation is represented by the broad apex at 1018.41 cm^{-1}, which is connected to the bone apogee of vibration at 839.03 cm^{-1} for the C-H vibration [22].

Fig. 2 presents the FTIR spectra of the CS: PVP blend, without and with various weight ratios of 7.5, 15, 22.5, 30, and 37.5 wt.% KI, labelled as (A1-A5). Following the incorporation of KI salt, the presence of polymer-salt interactions was confirmed through FTIR analysis, which inhibits the formation of hydrogen bonding between the chains. The observed variations in transmittance and the displacement of FTIR bands in the spectra indicate that the salt was thoroughly dissolved and complexed within the polymer composite. The complexity might be associated with alterations within the infrared range, including the emergence or disappearance on an infrared range and band shifting [23,24].

The FTIR spectral band assignments explain the polymer blend and their interactions at varying concentrations of KI wt.%. The analysis of the A0 spectra indicated that the characteristic absorption band at approximately 3263 cm^{-1} is linked to –OH and –NH stretching vibrations. The bands at 1556 cm^{-1} and 1645 cm^{-1} correspond to the –NH bending and C=O stretching, respectively. The –OH peak was observed at approximately 3261 cm^{-1}, as presented in Table 2.

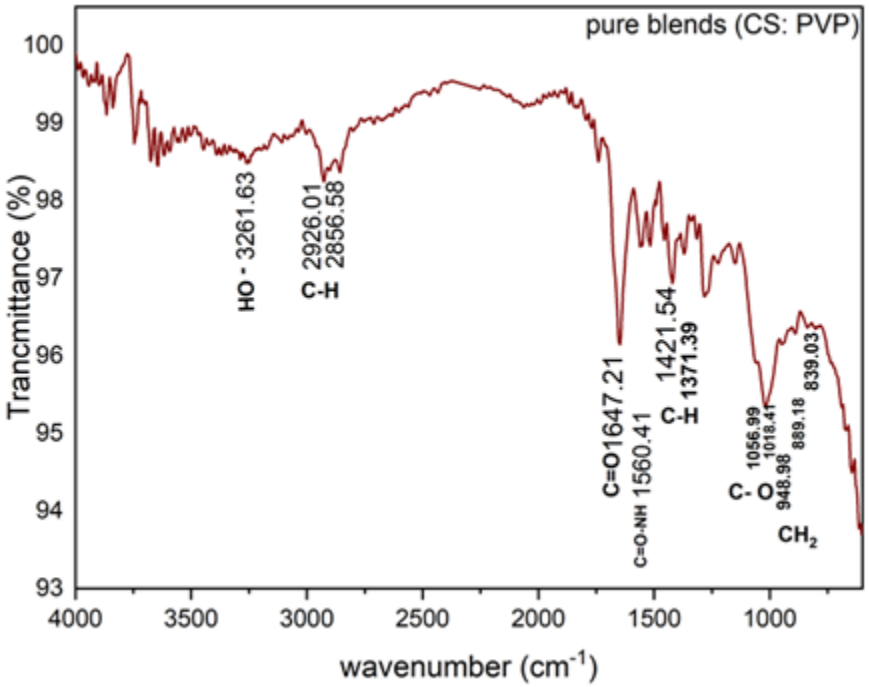

Figure 1: FTIR transmittance spectra of CS: PVP blend.

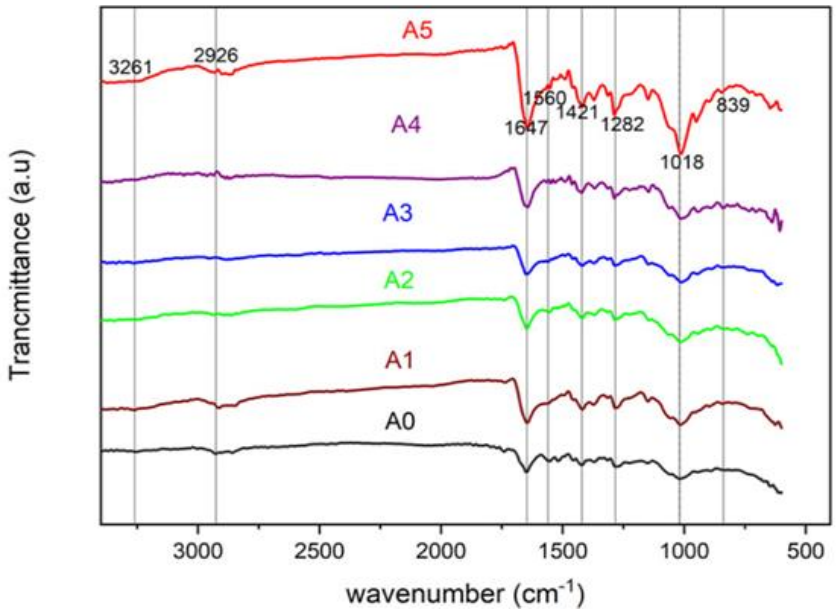

Figure 2: FTIR transmittance spectra of pure CS:PVP blend and CS:PVP with different wt.% KI.

Table 2: Characterization bands of the CS: PVP blend with different weight percentages of KI as determined by FTIR analysis.

Band Types	A0	A1	A2	A3	A4	A5
-OH Stretching/vibration	3261.63	3263.56	3197.98	3307.92	3419.79	3373.5
C-H stretching/vibration	2926.01	2914.44	2939.52	2866.22	2872.01	2870.08
C=O stretching/vibration	1647.21	1645.28	1645.28	1649.14	1643.35	1645.28
N-H bending amide	1560.41	1558.48	1556.55	1560.41	1548.84	1552.7
CH2 wagging vibration	1421.54	1419.61	1419.61	1419.61	1423.74	1419.61
C-O stretching / vibration	1282.66	1282.66	1284.59	1284.59	1286.52	1286.52
C-N stretching/vibration	1018.41	1016.49	1014.5	1010.7	1012.63	1012.63
C-H out of phase bending	839.03	842.89	833.04	839.03	840.96	844.82

3.2 UV-Vis Spectrophotometry

The optical behavior of materials can effectively be monitored using UV-visible absorption spectroscopy. The optical characteristics of matter are defined as any attribute that is related to the interaction between light and matter [25]. The absorbance spectra of the pure CS: PVP blend and that containing KI using a UV-Vis. spectrophotometer across the wavelength range of 200–1100 nm wavelength is depicted in Fig.3. All spectra exhibited a single absorption maximum at approximately 315 nm, which may be ascribed to the transparent nature of PVP and CS, consistent with previous studies [26].

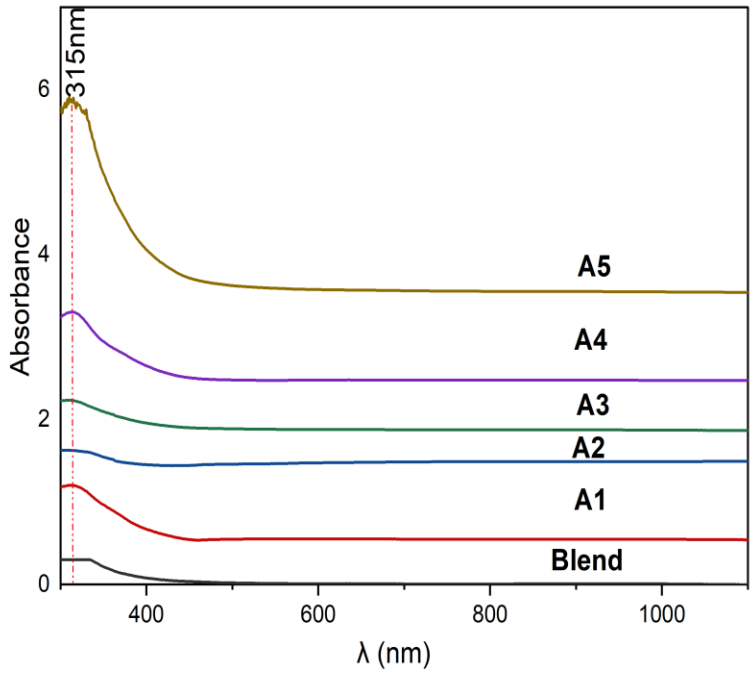

Figure 3: UV-Vis Absorbance spectra for CS: PVP polymer blend, and the polymer blend with different proportions of KI salt.

These peaks demonstrate that absorption occurs and intensifies with increasing KI concentration. This is a result of the interaction between the two mixtures CS:PVP, resulting in a slight increase in the wavelength and KI values.

The UV-Vis spectroscopy provides information on the energy gap of samples without and with KI as well as the molecular structures of organic substances. Two categories of semiconductors are commonly used: (1) direct bandgap and (2) indirect bandgap semiconductors [19]. UV-Vis spectroscopy can determine the absorption coefficient, optical band gap, and other optical parameters. The Beer-Lambert law, Eq.(1), is used to calculate the absorption coefficient from the optical absorption spectra.

$$\alpha(\nu) = 2.303\left(\frac{A}{L}\right) \quad \textbf{(1)}$$

where L denotes the film thickness in centimeters, A represents the absorbance, and α signifies the absorption coefficient [27]. Examining the absorption edge's spectral dependence is one approach to determine the optical bandgap (E_g). Fig. 4 illustrates the optical transitions linked to photon energies when $h\nu > E_g$. The current optical data can be assessed for near-edge optical absorption using the following relationship:

$$\alpha(\nu)h\nu = \beta\left(h\upsilon - E_g\right)^r \quad \textbf{(2)}$$

where α represents the extinction coefficient, h denotes Planck's constant, ν denotes the vibration frequency, A represents the absorption constant. The energy band gaps for the samples (A0-A1) were determined to be approximately 3.4, 3.2, 3.1, 3.09, 3.08 and 2.9 eV. These values were obtained through extrapolation of the linear part of $(\alpha h\nu)^2$ versus $(h\nu)$ curve [28]. The band gap energy values for samples without and with different wt% KI are presented in Table 3.

3.3 AC Conductivity

An inductance-capacitance-resistance (LCR) meter (Z Hi-tester, Nagano, Japan) was employed to perform Electrochemical Impedance Spectroscopy (EIS) for SPE over a frequency range of 50 Hz to 1 MHz. The 2.01 cm^2 electrolyte films were positioned between two stainless-steel electrodes and compressed under spring pressure. The stainless-steel electrode served as the working, reference, and counter electrodes [29]. The ionic conductivity (σ) of each sample was ascertained using the following equation:

$$\sigma = \frac{l}{R_b A} \quad \textbf{(3)}$$

where l, R_b and A denote the sample thickness, bulk resistance and electrode area, respectively. [30]. The impedance responses (Nyquist plots) for the CS: PVP polymer blend and the polymer blend with different proportions of KI salt are shown in Fig.5. The ionic conductivity and the bulk resistance for the different samples are listed in Table 4.

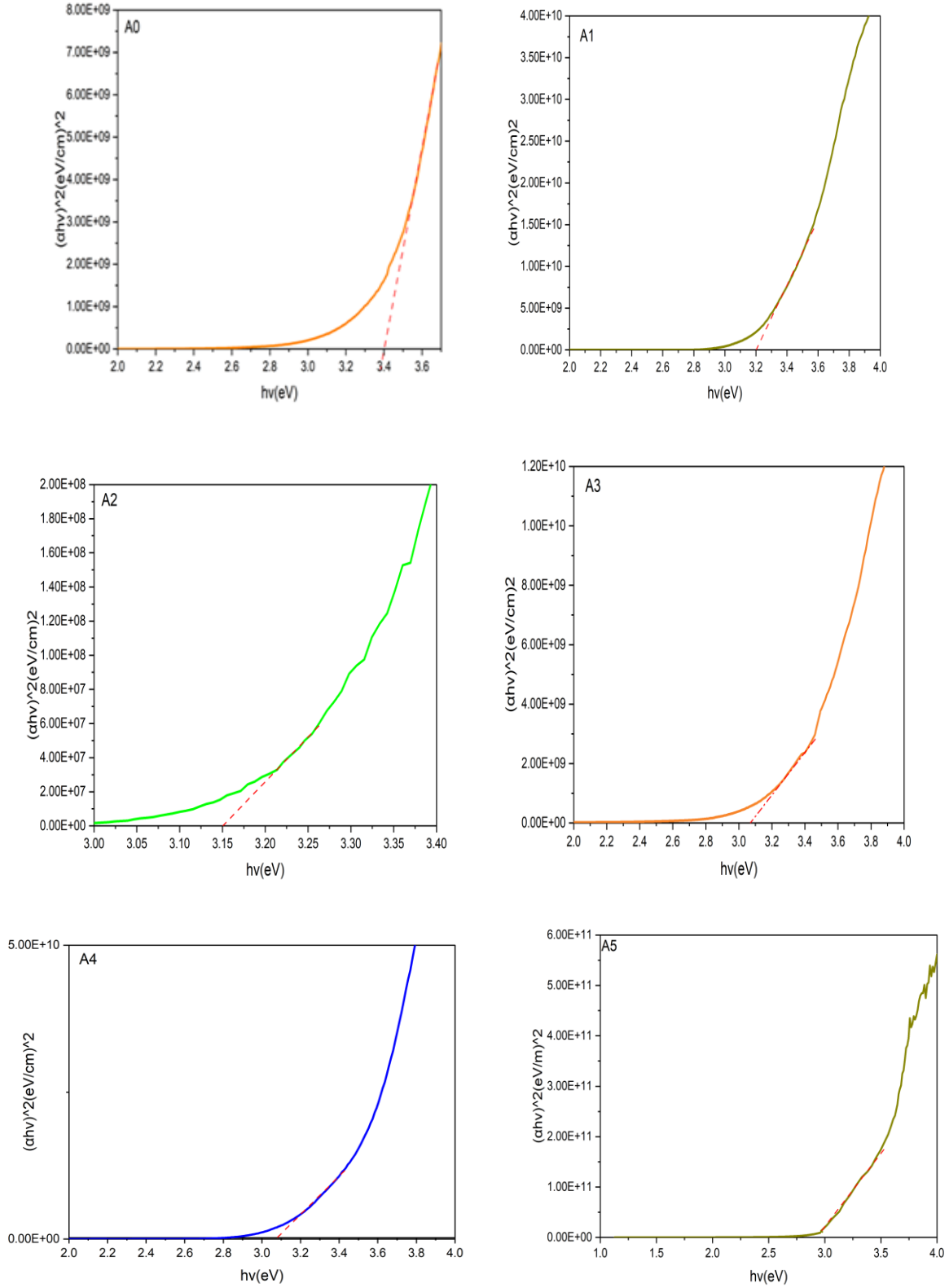

Figure 4: $(\alpha h\nu)^{1/2}$ and $(\alpha h\nu)^2$ versus photon energy hv (eV)for pure CS: PVP mixture, and the polymer blend with different proportions of KI salt.

Table 3: Band gap energy values for samples prepared with and without wt.% KI.

Assignment	$E_{.g.}$ (eV)
A0	3.4
A1	3.2
A2	3.1
A3	3.09
A4	3.08
A5	2.9

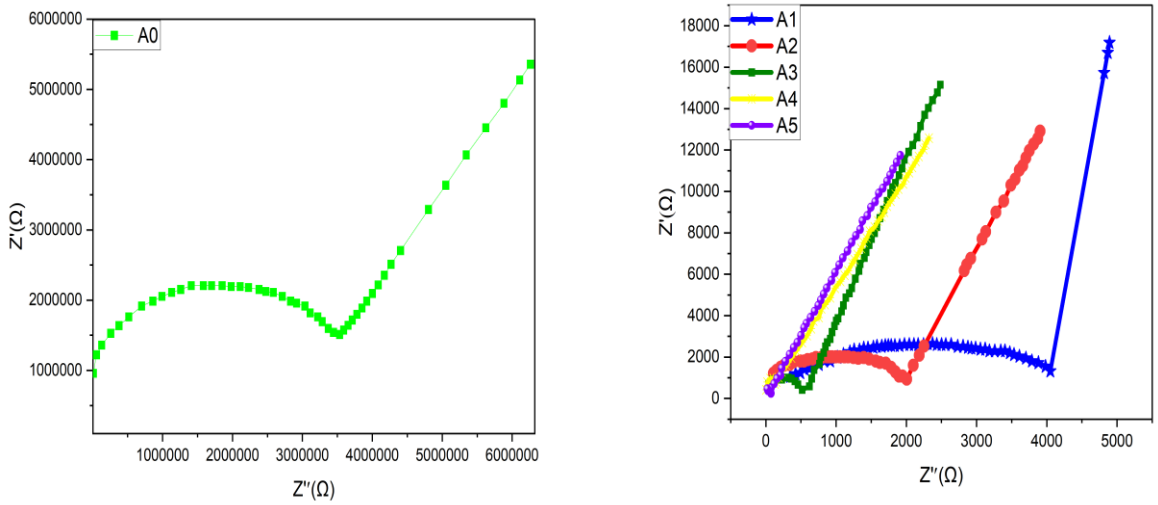

Figure 5: Nyquist plots for CS: PVP polymer blend, and the polymer blend with different proportions of KI salt.

Table 4: The conductivity, at room temperature of the films.

Assignment	$R_b(\Omega)$	Conductivity (S/cm)
A0	2560000	1.36×10^{-8}
A1	4000	4.5×10^{-6}
A2	2007.6	9×10^{-6}
A3	517.2	3.5×10^{-5}
A4	100	1.8×10^{-4}
A5	60	3×10^{-4}

Fig.6 illustrates the conductivity of the CS: PVP polymer blend and the polymer blend with different proportions of KI salt at 50 Hz. The ionic conductivity rises with increasing KI content, achieving a maximum of 3×10^{-4} S.cm^{-1} at 37.5 wt.% KI at room temperature. With an increase in KI concentration, the conductivity increases swiftly, which leads to an increase in free volume. This effect enhances the mobility of polymer fragments and the conductivity of ionic mobility [31].

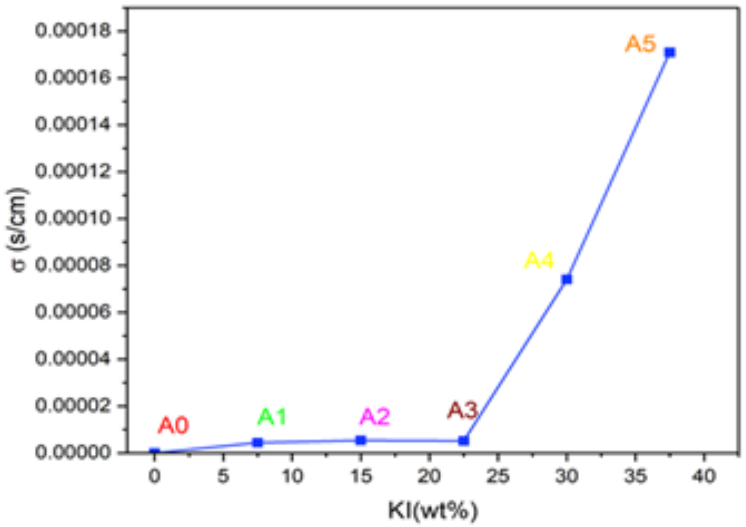

Figure 6: The ionic conductivity vs. different wt.% KI.

Fig. 7 illustrates the variations of the real dielectric constant (ε_r) for the electrolytes (A0-A5) at 25 ˚C with frequency of the range 50 Hz to 1 MHz. The real dielectric constant falls as the frequency increases due to an increase in conductivity. The real dielectric constant (ε_r) diminishes until it attains a plateau in the elevated frequency range [32]. This decrease in the dielectric constant at high frequencies is a result of the increase in dielectric dispersion. This phenomenon can be attributed to the behavior of polar materials, which initially have high true dielectric values. This can be explained by the fact that dipoles are unable to respond to rapid field changes at high frequencies, in addition to the presence of polarization effects. At high frequencies, the electric field also experiences rapid periodic reversals as a result of the absence of excess ion diffusion in the field's direction. Consequently, the real dielectric of all samples decreased as the frequency increased [30].

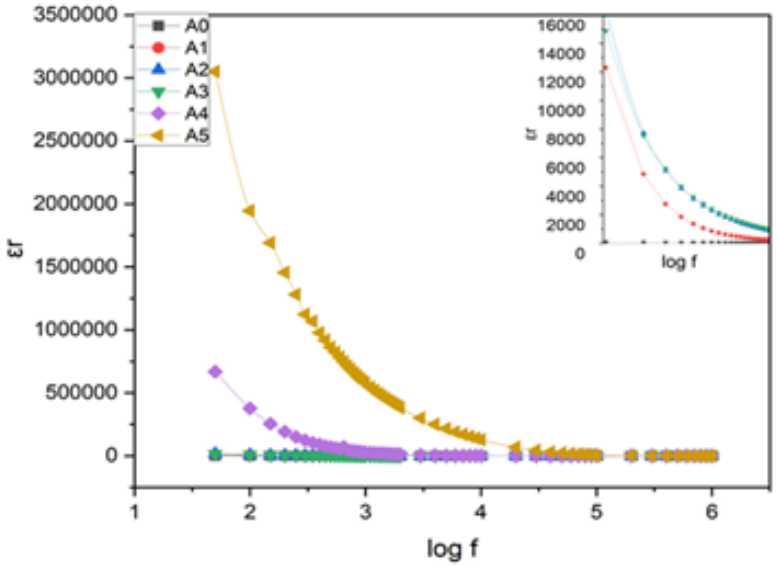

Figure 7: Variation of real part of dielectric constant with frequency for CS: PVP polymer blend and the polymer blend with different proportions of KI salt at room temperature.

4. Conclusions

Polymer electrolytes are considered among the most significant solid-state electrolytes. It is anticipated that the safety and energy density of lithium-ion batteries will be significantly enhanced through the use of polymer electrolytes. The mixture of CS: PVP in a 50:50 proportion was synthesized using the solution casting method with the addition of varying weight percentages of KI. The electrolyte measurements using Fourier transform infrared revealed a substantial interaction between polymer compounds CS: PVP and KI salts. In all samples, from the spectral analysis of UV- visible spectroscopy, the energy gap values decreased as the proportion of potassium iodide salt increased. The intensity, structure, and location of varying stretching modes are associated with interactions between polymer composites and KI in electrolytes. From the results of AC conductivity, the ionic conductivity increases with increasing KI salt concentration, the ionic conductivity of electrolyte A5 reached 3×10^{-4} S cm^{-1} at 37.5% KI salt. The real dielectric constant (ε_r) increases as the KI salt percentage increases. This behaviour can be ascribed to the dissociation of ions, which increases the number of available ions. Consequently, the complexity of ion movement is increased as the percentage of KI salt in a solution increases, resulting in a decrease in ionic conductivity and an increase in the true dielectric strength. Furthermore, the real dielectric constant decreased as the frequency increased. This behaviour is associated with the dissociation of the ions, which leads to their reduction because of their binding.

Conflict of Interest

Authors declare that they have no conflict of interest.

References

1. D. Wu and F-C Chang, Polymer, **48**, 989, (2007). https://doi.org/10.1016/j.polymer.2006.12.045.
2. J. Yue, M. Yan, Y. X. Yin, and Y. G. Guo, Advanced Functional Materials, **28**, (2018). https://doi.org/10.1002/adfm.201707533.
3. J. Schnell, T. Gunther, T. Knoche, C. Vieider, L. Köhler, A. Just, M. Keller, S. Passerini, and G. Reinhart, Journal of Power Sources, **382**,160, (2018). https://doi.org/10.1016/j.jpowsour.2018.02.062.
4. J. Janek and W. G. Zeier, Nature Energy, **1,** 16141, (2016).
5. L. Ye and X. Li, Nature, **593**, 218, (2021).
6. D. Zhang, X. Meng, W. Hou, W. Hu, J. Mo, T. Yang, W. Zhang, Q. Fan, L. Liu, B. Jiang, L. Chu, and M. Li, Nano Res. Energy, **2**, 1, (2023). https://doi.org/10.26599/NRE.2023.9120050.
7. S. Karthikeyan, S. Selvasekarapandian, M. Premalatha, S. Monisha, G. Boopathi, G. Aristatil, A. Arun, and S. Madeswaran, Springer Nature, **23**, 2775, (2017). https://doi.org/10.1007/s11581-016-1901-0.
8. H. Yang, Y. Liu, L. Kong, L. Kang, and F. Ran. Journal of Power Sources, **426**, 47, (2019). https://doi.org/10.1016/j.jpowsour.2019.04.023.
9. A. Z. Naser, I. Deiab, and B. M. Darras, RSC Adv., **11**, 17151, (2021). https://doi.org/10.1039/D1RA02390J.
10. M. L. Edward, K. C. Dharanibalaji, K. T. Kumar, A. R. S. Chandrabose, A. M. Shanmugharaj, and V. Jaisankar, Polymer Bulletin, **79**, 587, (2022). https://doi.org/10.1007/s00289-020-03472-1.
11. M. E. Ahmed, H. M. Mohamed, M. I. Mohamed, and N. G. Kandile, International Journal of Biological Macromolecules, **162**, 1388, (2020). https://doi.org/10.1016/j.ijbiomac.2020.08.048.
12. J. Park, S. Jo, N. Kitchamsetti, S. Zaman, and D. Kim, Journal of Alloys and Compounds, **926**, 166815, (2022). https://doi.org/10.1016/j.jallcom.2022.166815.
13. R. Kumar, I. Mishra, and G. Kumar, Journal of Polymers and the Environment, **29**, 1, (2021). https://link.springer.com/article/10.1007/s10924-021-02143-0.
14. P. Rawat, R. K. Prajapati, G. K. Meena, and A. L. Saroj, Materials Science and Engineering: B, **308**, 117603, (2024). https://doi.org/10.1016/j.mseb.2024.117603.
15. H. G. Rauf, J. M. Hadi, S. B. Aziz, R. T. Abdulwahid, and M. S. Mustafa, Int. J. Electrochem. Sci., **17**, 2, (2022), https://doi.org/10.20964/2022.05.04.

16. A. M. Zulkifli, N. Said, S. B. Aziz, E. Dannoun, S. Hisham, S. Shah, A. Abu Bakar, Z. H. Zainal, H. A. Tajuddin, J. M. Hadi, M. A. Brza, S. R. Saeed, and P. O. Amin, Molecules, **25**, 4115, (2020). https://doi.org/10.3390/molecules25184115.
17. M. K. Jawad, S. R. Majid, E. A. Al-Ajaj, and M. H. Suhail, Advances in Physics Theories and Applications, 34, 51, (2014).
18. R. T. Abdulwahid, S. B. Aziz, and M. F. Z. Kadir, Journal of Physics and Chemistry of Solids, **167**, 110774, (2022). https://doi.org/10.1016/j.jpcs.2022.110774.
19. A. M. Abdelghany, M. S. Meikhail, A. H. Oraby, and M. A. Aboelwafa, Polymer Bulletin, **80**, 13279, (2023). https://doi.org/10.1007/s00289-023-04700-0.
20. F. F. Awang, M. F. Hassan, and K. H. Kamarudin, Ionics, **28**, 1249, (2022).
21. A Safo, M. Werheid, C. Dosche, and M. Oezaslan, Nanoscale Adv., **1**, 3095, (2019). https://doi.org/10.1039/C9NA00186G.
22. L. A. Jassim and M. K. Jawad, Iraqi Journal of Applied Physics, **20**, 61, (2024).
23. K. Deshmukh, M. Ahamed, K. Sadasivuni, D. Ponnamma, M. Al-Ali A. Rajendra, R. Deshmukh, S. Pasha, A. Polu, and K. Chidambaram, Journal of Applied Polymer Science, **134**, (2017). https://doi.org/10.1002/app.44427.
24. J. O. Dennis, A. A. Adam, M. K. M. Ali, H. Soleimani, M. F. B. A. Shukur, K. H. Ibnaouf, O. Aldaghr, M. H. Eisa, M. A. Ibrahem, A. B. Abdulkadir, and V. Cyriac, Membranes, **12**, 706, (2022). https://doi.org/10.3390/membranes12070706.
25. N. J. Abdullah, A. F. Essa, and S. M. Hasan, Iraqi Journal of Science, **62**, 138, (2021). https://doi.org/10.24996/ijs.2021.62.1.13.
26. A. M. Elashmawi, A. M. Abdelghany, and N. A. Hakeem, Journal of Materials Science, **24**, 2956, (2013). https://doi.org/10.1007/s10854-013-1197-z.
27. G. M. Asnag, A. H. Oraby, and A. M. Abdelghany, Composites Part B: Engineering, **172**, 436, (2019). https://doi.org/10.1016/j.compositesb.2019.05.044.
28. A. A. Essawy, M. F. Hussein, T. H. A. Hasanin, E. F. El Agammy, H. S. Alsaykhan, R. F. Alanazyi, and A. El Essawy, Ceramics, **7**, 1100, (2024). https://doi.org/10.3390/ceramics7030072.
29. M. M. Nofal, J. M. Hadi, S. B. Aziz, M. A. Brza, A. S. Asnawi, E. M. Dannoun, A. M. Abdullah, and M. F. Kadir, Materials, **14**, 4859, (2021). https://doi.org/10.3390/ma14174859.
30. M. K. Jawad and F. M. Ahmed, Journal of Theoretical and Applied Physics, **18**, 1 (2024). https://doi.org/10.57647/j.jtap.2024.si-AICIS23.23.
31. F. M. Ahmed and M. K. Jawad, Iraqi Journal of Physics, **21**, 1, (2023). https://doi.org/10.30723/ijp.v21i1.1093.
32. E. A. Swady and M. K. Jawad, *AIP Conf. Proc.* 2437, 020053 (2022), https://doi.org/10.1063/5.0092661.

الخواص البصرية والكهربائية للالكتروليت البوليمري الصلب الذي أساسه بوليمر طبيعي

الاء مناف قصي[1] ومحمد كاظم جواد[1]
[1]قسم الفيزياء، كلية العلوم، جامعة بغداد، بغداد، العراق

الخلاصة

الإلكتروليتات البوليمرية الحيوية المكونة من خليط طبيعي والذي يكون مانع للتسرب، يتحلل بيولوجيا، مرن، يدرس بشكل واسع. الكتروليت البوليمر الحيوي المستخدم في هذه الدراسة مكون من نسبة ثابته من الكيتوسان والبولي فينيل بايروليدون (CS: PVP) (50: 50) وينسب وزنية مختلفة من ملح البوتاسيوم KI(7.5,15,22.5.30.37.5) قد تم تحضيره باستخدام تقنية صب المحلول. تم توصيف النماذج باستخدام مطياف الاشعة فوق البنفسجة UV-vis، تحويلات الاشعة تحت الحمراء FTIR, والتوصيلية الكهربائية المستمرة AC Conductivity . أن التداخل ما بين الخليط البوليمري (CS: PVP) وملح البوتاسيوم تم تأكيده بواسطة دراسة تحويلات الاشعة تحت الحمراء FTIR. أن إضافة ملح البوتاسيوم من المحتمل ان يكون المسبب لحدوث التفاعل ما بين الملح والبوليمر، هذا سوف يمنع تكوين اصرة هيدروجينية ما بين السلاسل. تم ملاحظة وجود قمة امتصاص واحدة فقط من خلال مطياف الاشعة فوق البنفسجية للنموذج تقريبا عند عدد موجي 315nm. مع زيادة النسبة الوزنية لملح البوتاسيوم ارتفعت التوصيلية حتى وصلت $3\times10^{-4}Scm^{-1}$ عند درجة حرارة الغرفة للنموذج الذي يحتوي 37.5 wt.% من ملح البوتاسيوم.

الكلمات المفتاحية: خليط بوليمري حيوي، ملح البوتاسيوم، الخواص البصرية، التوصيلية الايونية للتيار المستمر، إلكتروليتات البوليمر الحيوي الصلبة.